



Anomalous sign inversion of spin-orbit torque in ferromagnetic/nonmagnetic bilayer systems due to self-induced spin-orbit torque

Motomi Aoki,¹ Ei Shigematsu,¹ Ryo Ohshima ,¹ Teruya Shinjo,¹ Masashi Shiraishi ,¹ and Yuichiro Ando^{1,2,*}

¹*Department of Electronic Science and Engineering, Kyoto University, Kyoto, Kyoto 615-8510, Japan*

²*PRESTO, Japan Science and Technology Agency, Honcho, Kawaguchi, Saitama 332-0012, Japan*



(Received 9 November 2021; revised 1 November 2022; accepted 4 November 2022; published 17 November 2022)

Self-induced spin-orbit torques (SI-SOTs) in ferromagnetic (FM) layers have been overlooked when estimating the spin Hall angle (SHA) of adjacent nonmagnetic (NM) layers. In this work, we observe anomalous sign inversion of the total SOT in the spin-torque ferromagnetic resonance due to the enhanced SI-SOT, and successfully rationalize the sign inversion through a theoretical calculation considering the SHE in both the NM and FM layers. The findings show that using an FM layer whose SHA sign is the same as that of the NM achieves efficient SOT-magnetization switching with the assistance of the SI-SOT. The contribution of the SI-SOT becomes salient for a weakly conductive NM layer, and conventional analyses that do not consider the SI-SOT can overestimate the SHA of the NM layer by a factor of more than 150.

DOI: [10.1103/PhysRevB.106.174418](https://doi.org/10.1103/PhysRevB.106.174418)

I. INTRODUCTION

The spin Hall effect (SHE) [1] in a nonmagnetic (NM) material with a sizable spin-orbit interaction (SOI) realizes injection of a pure spin current into an adjacent ferromagnetic (FM) material and exerts torque on the magnetization via spin-orbit torque (SOT) [2], which enables manipulation and even switching of the magnetization [3–10]. Efficient generation of SOT requires a material with a large spin Hall angle (SHA). Because the magnitude of SOI is roughly proportional to the fourth power of the atomic number, most research on SOT has focused on materials containing heavy elements [5,7,11,12]. Highly efficient charge-to-spin conversion has been discovered in platinum (Pt), tungsten (W), and tantalum (Ta) [5,6,11]. Such studies have generally used FM/NM bilayer systems to directly detect the SOT. However, most of these studies have overlooked a non-negligible contribution: the self-induced spin-orbit torque (SI-SOT), which originates from the spin Hall effect in the FM layer itself. Furthermore, recent studies have revealed that charge-to-spin conversion efficiency in 3D FM layers is substantially high despite their relatively small atomic numbers [13–16], and the SHE of the FM layer can exert SOT on the FM magnetization itself in an NM/FM bilayer [17–19]. Nevertheless, experimental studies have not addressed non-negligible SI-SOT in the FM layer and SOT from the adjacent NM layer separately. This hampers precise estimation of the SHA of the NM layer, because SOT applied to the FM layer is a combination of the aforementioned SOTs with different physical origins.

In this paper, we demonstrate anomalous sign inversion of the SOT in NM/FM bilayer devices in spin-torque ferromagnetic resonance (ST-FMR) [11], which is caused by enhanced SI-SOT. Since the SI-SOT (scaled by the spin-dephasing

length in the FM) and SOT from the NM layer (scaled by the spin-diffusion length in the NM) exhibit different thickness dependences, these contributions can be separated by measuring the ST-FMR signals with a wide range of thickness of the FM layer, t_{FM} . The t_{FM} dependence of the total SOT was well reproduced by a theoretical model considering the SHE in both the NM and FM layers [20]. Consequently, the SI-SOTs are -43 and 27% of the SOT from the NM layer in Ta(5 nm)/Co(5 nm) and permalloy(5 nm)/Pt(5 nm) bilayers, respectively, which are both large. Our findings reveal that combining FM and NM layers with the same SHA sign achieves efficient SOT-magnetization switching, because the SI-SOT augments the efficiency. More importantly, the SI-SOT contribution becomes dominant for a weakly conductive NM layer, and the conventional analyses of the SOT in NM/FM bilayer systems that do not consider SI-SOT can overestimate the SHA of the NM layer by a factor of more than 150. Our study provides a fuller understanding of conventional SOT physics.

II. EXPERIMENTAL PROCEDURES

Figure 1(a) shows a schematic of the device structure and the electrical circuit used in our study. Rectangular $10\ \mu\text{m} \times 25\ \mu\text{m}$ Ta(t_{NM})/Co(t_{FM})/SiO₂(7 nm) channels were fabricated on MgO (001) substrates using rf-magnetron sputtering, where t_{NM} was fixed to 5 nm and t_{FM} was varied from 3 to 17.5 nm. Hereafter, number in bracket indicates thickness in the unit of nanometers. In the ST-FMR experiments, a DC voltage, V_{DC} , was measured under an introduced microwave AC current using a commercial analog signal generator via a Ti(3)/Au(70) coplanar waveguide. The angle θ , between the external magnetic field H_{ext} and the x axis, was changed from 0° to 360° . All measurements were carried out at room

*ando.yuichiro.5s@kyoto-u.ac.jp

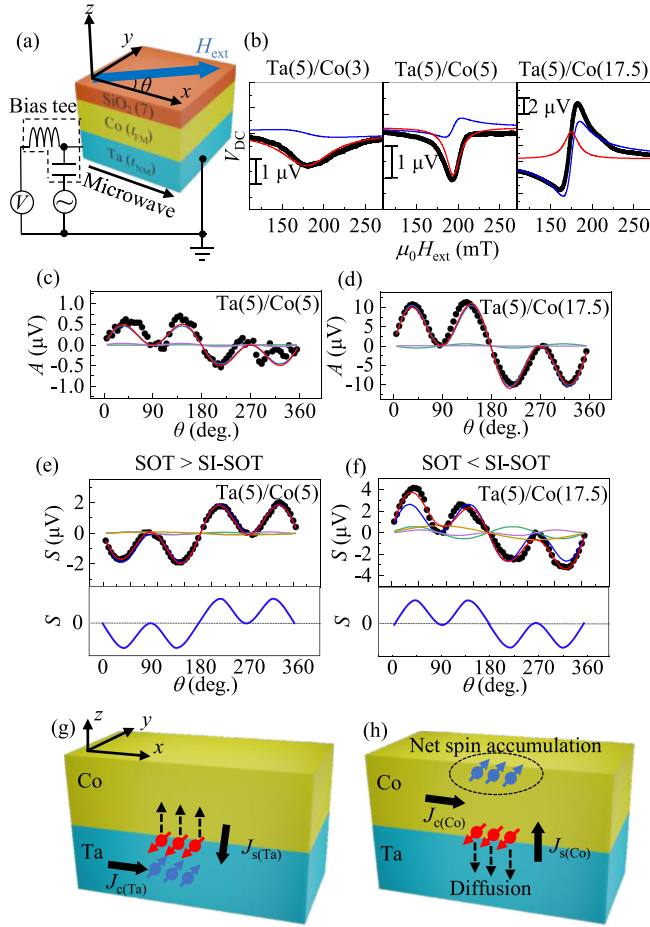


FIG. 1. (a) Schematic of the device structure and the electrical circuit. (b) ST-FMR spectra of (left panel) Ta(5)/Co(3), (middle panel) Ta(5)/Co(5), and (right panel) Ta(5)/Co(17.5) devices. Red and blue curves show the symmetric and the antisymmetric component obtained by fitting with Eq. (1). (c), (d) Measured θ dependence of A of (c) Ta(5)/Co(5) and (d) Ta(5)/Co(17.5) devices. (e), (f) Upper panel) Measured and (lower panel) expected θ dependence of S of (e) Ta(5)/Co(5) and (f) Ta(5)/Co(17.5) devices. Solid lines are the total fitting (red), $\sin 2\theta \cos \theta$ (blue), $\sin 2\theta$ (green), $\sin 2\theta \sin \theta$ (purple), and $\sin \theta$ (brown) terms. (g), (h) Schematics of the spin injection into Co via the SHE in (g) Ta and (h) Co. In the ST-FMR measurements, frequency, f , was 13 GHz when $t_{\text{FM}} = 3$ nm and 16 GHz when $t_{\text{FM}} \geq 5$ nm. Signal output power was fixed to 13 dBm.

temperature. V_{DC} is expressed as [11]

$$V_{\text{DC}} = A \frac{\Delta(\mu_0 H_{\text{ext}} - \mu_0 H_{\text{FMR}})}{(\mu_0 H_{\text{ext}} - \mu_0 H_{\text{FMR}})^2 + \Delta^2} + S \frac{\Delta^2}{(\mu_0 H_{\text{ext}} - \mu_0 H_{\text{FMR}})^2 + \Delta^2}, \quad (1)$$

where A and S are the magnitudes of the antisymmetric and the symmetric Lorentzian functions, respectively, Δ is the half-width at half maximum, μ_0 is the vacuum permeability, and H_{FMR} is the ferromagnetic resonance field. Here, we use the definition of FMR spin-torque efficiency, ξ_{FMR} , which has been considered to be close to the SHA of the NM layer,

as [11]

$$\xi_{\text{FMR}} = \frac{S e \mu_0 M_S t_{\text{NM}} t_{\text{FM}}}{A \hbar} \sqrt{1 + \frac{M_{\text{eff}}}{H_{\text{FMR}}}}, \quad (2)$$

where e , M_S , M_{eff} , and \hbar are the elementary charge, saturation magnetization, effective magnetization, and Dirac constant, respectively. M_{eff} was obtained from the $H_{\text{FMR}}-f$ curve using the Kittel formula [21], and $\mu_0 M_S$ for Co was determined to be 1.87 T from the linear fit of the $1/M_{\text{eff}}-1/t_{\text{FM}}$ plot [22] (see Supplemental Material (SM), Sec. A [23]).

III. SPIN-TORQUE FERROMAGNETIC RESONANCE MEASUREMENT ON Ta/Co BILAYERS

Figure 1(b) shows the ST-FMR spectra for $t_{\text{FM}} = 3$ (left), 5 (middle), and 17.5 nm (right) when $\theta = 45^\circ$. The red (blue) curves are the symmetric (antisymmetric) components of the spectra obtained by fitting with Eq. (1). When the SI-SOT is negligible, the sign of $A(S)$ is positive (negative) in our setup, considering the direction of the Oersted field and the negative SHA of Ta. The signs of both A and S in Ta(5)/Co(5) agree with the expectation. In Ta(5)/Co(3), the sign of A was inverted owing to the contribution from the fieldlike SOT [24], but the sign of S was negative as in Ta(5)/Co(5). A significant result is in the ST-FMR spectrum of Ta(5)/Co(17.5), where the sign of S was surprisingly inverted by simply increasing the Co thickness [see the right panel of Fig. 1(b)]. To reveal t_{FM} dependence of the spin torque in detail, θ dependences of ST-FMR signals were measured. Table I summarizes possible angular dependences in antisymmetric (A) and symmetric (S) component in the ST-FMR spectrum, where \mathbf{M} is the magnetization vector [25,26]. Under the experimental setup shown in Fig. 1(a), Oersted field along the y direction and SOT from σ_y spins via the SHE in Ta and Co are expected to be dominant contributions. Both Oersted field along the y direction and fieldlike (FL) SOT due to σ_y spins contribute to $\sin 2\theta \cos \theta$ term in A , while dampinglike (DL) SOT due to σ_y spins contribute to $\sin 2\theta \cos \theta$ term in S . Though other contributions such as Oersted field along the x and z directions are also expected, they do not appear in $\sin 2\theta \cos \theta$ term of S . Because the inverse spin Hall effect induced by spin pumping (SP-ISHE) and anomalous Nernst effect (ANE) are negligible in Ta/Co bilayers used in our study, as discussed later, ξ_{FMR} is estimated more precisely by using $A(S)_{\sin 2\theta \cos \theta}$ as $A(S)$ in Eq. (2), where $A(S)_{\sin 2\theta \cos \theta}$ is $\sin 2\theta \cos \theta$ term in $A(S)$. Figures 1(c) and 1(d) show θ dependence of A , while the upper panels in Figs. 1(e) and 1(f) show θ dependences of S for Ta(5)/Co(5) and Ta(5)/Co(17.5), respectively, where solid lines are total fitting (red), $\sin 2\theta \cos \theta$ (blue), $\sin 2\theta$ (green), $\sin 2\theta \sin \theta$ (purple), and $\sin \theta$ (brown) term (see Table I). Schematics of expected $\sin 2\theta \cos \theta$ component in S with negative and positive SOTs are also exhibited in the lower panels of Figs. 1(e) and 1(f), respectively. Whereas the sign of $A_{\sin 2\theta \cos \theta}$ was identical in both cases, the sign of $S_{\sin 2\theta \cos \theta}$ was actually inverted for $t_{\text{FM}} = 17.5$ nm, which cannot be explained in the conventional ST-FMR framework.

To explain the anomalous spin inversion in $\sin 2\theta \cos \theta$ component in S , shown in Figs. 1(e) and 1(f), contribu-

TABLE I. Origin of the angular dependencies of (a) A and (b) S . σ_i indicates spin polarization of injected spin current.

(a) A component				
θ dependence	$\sin 2\theta \cos \theta$		$\sin 2\theta$	$\sin 2\theta \sin \theta$
Torque form	$\mathbf{y} \times \mathbf{M}$		$\mathbf{M} \times (\mathbf{M} \times \mathbf{z})$	$\mathbf{x} \times \mathbf{M}$
Origin	FL torque due to σ_y		DL torque due to σ_z	FL torque due to σ_x
Oersted field	y			x
Undesired effect				
(b) S component				
θ dependence	$\sin 2\theta \cos \theta$	$\sin 2\theta$	$\sin 2\theta \sin \theta$	$\sin \theta$
Torque form	$\mathbf{M} \times (\mathbf{M} \times \mathbf{y})$	$\mathbf{z} \times \mathbf{M}$	$\mathbf{M} \times (\mathbf{M} \times \mathbf{x})$	
Origin	DL torque due to σ_y	FL torque due to σ_z	DL torque due to σ_x	
Oersted field		z		
Undesired effect	SP-ISHE and ANE			SP-ISHE

tion of the spin Hall effect in the Co layer is considered. Figure 1(g) shows a schematic of spin-current generation via the SHE of Ta with a negative SHA in the Ta/Co bilayer. The electric current in the Ta layer along the $+x$ direction, $J_{c(\text{Ta})}$, is converted into the spin current along the $-z$ direction, $J_{s(\text{Ta})}$, via the SHE in the Ta layer, resulting in the negative SOT. Here, negative (positive) SOT is defined to be the SOT that aligns the magnetization along the $+(-)y$ direction. Note that the electric shunting current through the Co layer is a function of the conductance ratio between the Co and Ta layers, yielding spin current via the SHE of Co. The electric current shunting into the Co layer along the $+x$ direction, $J_{c(\text{Co})}$, is converted into the spin current along the $+z$ direction, $J_{s(\text{Co})}$ [see Fig. 1(h)]. In the case of a single Co layer without adjacent NM layers, spins with opposite directions ($+y$ and $-y$) accumulate on the top and the bottom surfaces, and they cannot flow out from the Co layer. Consequently, the net sum of the spin accumulations in the Co layer is zero. In contrast, in the case of the Ta/Co bilayer, spins accumulated at the Ta/Co interface can diffuse into the Ta layer through the Ta/Co interface, and a net spin accumulate at the top interface, generating SI-SOT with positive polarity. The amount of the SOT of the NM layer and the SI-SOT depends on $t_{\text{NM}}/l_{\text{NM}}$, and the $t_{\text{FM}}/l_{\text{FM}}$, respectively, as well as the SHA of the NM and FM layer, where $l_{\text{NM(FM)}}$ is the spin-diffusion (dephasing) length of the NM (FM). Thus, the experimentally detected SOT, i.e., the net SOT, can be controlled by changing t_{FM} . Increasing t_{FM} allows the cancellation of the SOT of the NM layer by

the SI-SOT, and the anomalous sign inversion in $\sin 2\theta \cos \theta$ component in S .

IV. THEORETICAL ANALYSIS OF THICKNESS DEPENDENCE OF ξ_{FMR} USING THE SPIN-DIFFUSION MODEL

Figure 2(a) shows ξ_{FMR} obtained from θ dependence of the ST-FMR spectra as a function of t_{FM} for the various Ta/Co bilayers. ξ_{FMR} at $t_{\text{FM}} = 3$ nm is positive because of negative A , which is attributed to the fieldlike SOT [24]. Above $t_{\text{FM}} = 5$ nm, ξ_{FMR} is negative because of positive A due to dominant contribution of the Oersted field, and negative S . Importantly, ξ_{FMR} becomes positive again at $t_{\text{FM}} \geq 8.5$ nm owing to the sign reversal of S , which is attributed to the SI-SOT. Because both the DL torque efficiency, ξ_{DL} , and FL torque efficiency, ξ_{FL} , are known to have negligible dependence on t_{FM} in the conventional understanding, $1/\xi_{\text{FMR}}$ is expected to be linearly proportional to $1/t_{\text{FM}}$. This has been used to estimate ξ_{DL} and ξ_{FL} from the linear fit of the $1/\xi_{\text{FMR}} - 1/t_{\text{FM}}$ plot [24,27,28]. However, the results in Fig. 2(b) show a noticeable nonlinear dependence of $1/\xi_{\text{FMR}}$ on $1/t_{\text{FM}}$. Thus, we calculated ξ_{FMR} using the spin-diffusion equation [20] applying the following boundary conditions: continuity of the spin chemical potential and spin current at the NM/FM interface, and zero spin current at the top and bottom of the NM/FM bilayer. The total spin current with a spin vector transverse to the magnetization at the NM/FM interface, $J_{s\perp}$, is expressed as

$$J_{s\perp} = \frac{\tanh\left(\frac{t_{\text{NM}}}{2l_{\text{NM}}}\right)R_{s(\text{NM})}J_{c(\text{NM})}\theta_{\text{NM}} + \tanh\left(\frac{t_{\text{FM}}}{2l_{\text{FM}}}\right)R_{s(\text{FM})}J_{c(\text{FM})}\theta_{\text{FM}}}{R_{s(\text{NM})} \coth\left(\frac{t_{\text{NM}}}{l_{\text{NM}}}\right) + R_{s(\text{FM})} \coth\left(\frac{t_{\text{FM}}}{l_{\text{FM}}}\right)} \sin\theta. \quad (3)$$

Here, θ_{NM} (θ_{FM}) is the SHA of the NM (FM) layer, and $R_{s(\text{NM})}$ ($R_{s(\text{FM})}$) $\equiv l_{\text{NM(FM)}}/\sigma_{\text{NM(FM)}}$ is the spin resistance of the NM (FM) layer, where $\sigma_{\text{NM(FM)}}$ is the conductivity of the NM (FM) layer. For simplicity, we neglect the interfacial spin-orbit coupling and the spin precession during the diffusion [29], i.e., $\xi_{\text{DL}} = J_{s\perp}/(J_{c(\text{Ta})} \sin \theta)$, and thus, Eq. (3) is the simplified expression of the generalized formalism described in Ref. [18]. Such a simplification does not affect our main results because the contribution of the interfacial spin-orbit coupling is much

less dependent on NM and FM thicknesses. Consequently, ξ_{FMR} is expressed as [27]

$$\xi_{\text{FMR}} = \left\{ \frac{R_{s(\text{NM})} \coth\left(\frac{t_{\text{NM}}}{l_{\text{NM}}}\right) + R_{s(\text{FM})} \coth\left(\frac{t_{\text{FM}}}{l_{\text{FM}}}\right)}{\tanh\left(\frac{t_{\text{NM}}}{2l_{\text{NM}}}\right)R_{s(\text{NM})}\theta_{\text{NM}} + \tanh\left(\frac{t_{\text{FM}}}{2l_{\text{FM}}}\right)R_{s(\text{FM})}\frac{\sigma_{\text{FM}}}{\sigma_{\text{NM}}}\theta_{\text{FM}}} + \frac{\hbar}{e\mu_0 M_S t_{\text{NM}} t_{\text{FM}}} \frac{\xi_{\text{FL}}}{\xi_{\text{DL}}} \right\}^{-1}. \quad (4)$$

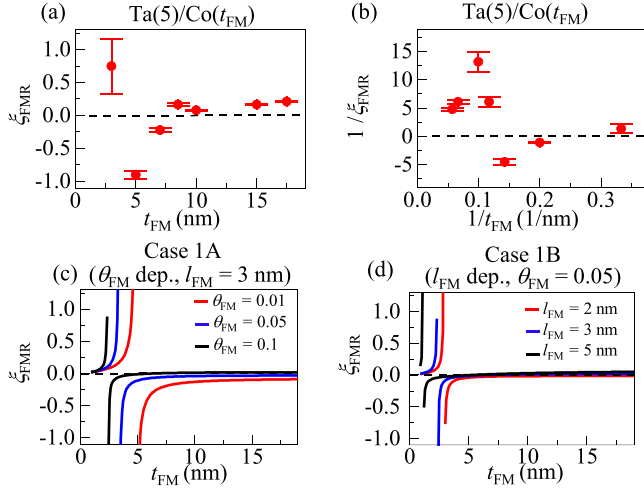


FIG. 2. (a) ξ_{FMR} as a function of t_{FM} and (b) $1/\xi_{\text{FMR}}$ as a function of $1/t_{\text{FM}}$ for Ta/Co devices. (c) θ_{FM} and (d) l_{FM} dependences of the $\xi_{\text{FMR}}-t_{\text{FM}}$ curve for case 1.

Figures 2(c) and 2(d) show ξ_{FMR} calculated as a function of t_{FM} for Ta/Co for (c) various values of θ_{FM} (0.01, 0.05, and 0.1) and fixed l_{FM} (3 nm) (case 1A), and (d) fixed θ_{FM} (0.05) and various l_{FM} (2, 3, and 5 nm) (case 1B) [30,31]. Here, we used literature values of l_{NM} and θ_{NM} [5,32], and the measured values for σ_{NM} and σ_{FM} (case 1 in Table II). Although θ_{FM} measured using the spin valve is on the order of 0.01 [15], it is on the order of 0.1 from the measurement of the anomalous spin-orbit torque [31] and the theoretical calculation [33]. Therefore, θ_{FM} should be varied from 0.01 to 0.1. Considering that the reported values of $\xi_{\text{FL}}/\xi_{\text{DL}}$ are from -1 to 1 [24,27] and the fieldlike SOT is large enough to cancel the Oersted field when $t_{\text{FM}} < 3$ nm, we set $\xi_{\text{FL}}/\xi_{\text{DL}} = 1$ for the Ta/Co. Both cases 1A and 1B qualitatively reproduce the experimental results obtained from ST-FMR as shown in Fig. 2(a): the sign reversal of ξ_{FMR} appearing in the thin and thick regimes is related to the fieldlike SOT and the SI-SOT, respectively. Using $\theta_{\text{FM}} = 0.05$, $\theta_{\text{NM}} = -0.15$, $l_{\text{FM}} = 3$ nm, and $l_{\text{NM}} = 1.8$ nm, we find the SI-SOT contribution to ξ_{DL} in the Ta(5)/Co(5) sample is approximately -43% (the negative sign indicates suppression of the SOT from Ta) of that of the SOT arising from Ta, indicating that the SI-SOT largely hampers the SOT from the Ta layer. The presence or absence of the sign reversal of ξ_{FMR} from negative to positive strongly depends on the values of θ_{FM} , θ_{NM} , l_{FM} , and l_{NM} . The conditions for the sign reversal are large θ_{FM} and l_{FM} , and small θ_{NM} and l_{NM} , because larger θ_{FM} results in more efficient spin-current generation in the FM layer and larger l_{FM} is equivalent to a higher spin resistance of the FM layer. This

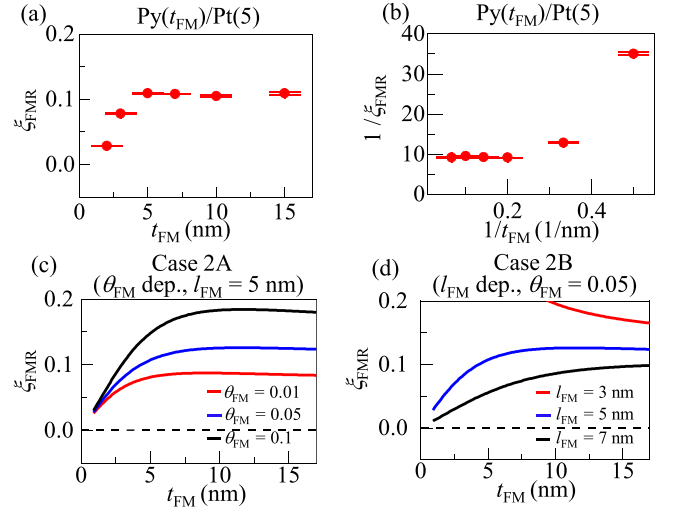


FIG. 3. (a) ξ_{FMR} as a function of t_{FM} and (b) $1/\xi_{\text{FMR}}$ as a function of $1/t_{\text{FM}}$ for Py/Pt devices. (c) θ_{FM} and (d) l_{FM} dependences of the $\xi_{\text{FMR}}-t_{\text{FM}}$ curve for case 2. $f = 13$ GHz, 11 GHz, and 5 GHz when $t_{\text{FM}} \geq 10$ nm, $7 \text{ nm} \geq t_{\text{FM}} \geq 3$ nm, and $t_{\text{FM}} = 3$ nm, respectively. Signal output power was fixed to 13 dBm.

enhances the spin-current flow from the FM to the NM layer. The small θ_{NM} and l_{NM} also contribute to the SOT suppression and low spin resistance of the NM layer, respectively.

V. CONTROL EXPERIMENTS AND CONTRIBUTION OF SPURIOUS EFFECTS

To obtain further evidence, we investigated the thickness dependence of ξ_{FMR} for permalloy ($\text{Ni}_{81}\text{Fe}_{19}$, Py)/Pt bilayers because no anomalous sign inversion is expected owing to positive θ_{NM} and θ_{FM} . Figures 3(a) and 3(b) show ξ_{FMR} and $1/\xi_{\text{FMR}}$ as functions of t_{FM} and $1/t_{\text{FM}}$, respectively, for Py (t_{FM})/Pt (5 nm). Sign inversion of ξ_{FMR} indeed was not observed up to $t_{\text{FM}} = 15$ nm. Meanwhile, the $1/\xi_{\text{FMR}}-1/t_{\text{FM}}$ plot does not exhibit a linear relationship as shown in Fig. 3(b). Calculating ξ_{FMR} using Eq. (4) well reproduces the experimental result even for thin and thick t_{FM} regions [see Figs. 3(c) and 3(d) and Table II (case 2) for the calculation parameters]. Using $\theta_{\text{FM}} = 0.05$, $\theta_{\text{NM}} = 0.32$, $l_{\text{FM}} = 5$ nm, and $l_{\text{NM}} = 1.4$ nm, we estimate the contribution of SI-SOT to ξ_{DL} in the Py(5)/Pt(5) sample to be $+27\%$ of that of the SOT from Pt, indicating that the SI-SOT assists the original SOT from the Pt layer. Importantly, the enhancement of ξ_{FMR} for larger θ_{FM} in Fig. 3(c) shows that selecting an FM layer with a large θ_{FM} that has the same sign as θ_{NM} achieves efficient SOT generation with assistance from the SI-SOT.

TABLE II. Parameters used in the various cases calculated with Eq. (4).

Case	$\sigma_{\text{NM}} (\times 10^4 (\Omega \text{ m})^{-1})$	$\sigma_{\text{FM}} (\times 10^4 (\Omega \text{ m})^{-1})$	l_{NM} (nm)	l_{FM} (nm)	θ_{NM}	θ_{FM}	$\xi_{\text{FL}}/\xi_{\text{DL}}$
1	43	101	1.8 [5]	2–5	-0.15 [5]	0.01–0.1	1
2	176	182	1.4 [27]	3–7	0.32 [27]	0.01–0.1	-0.2
3	176	101	3	5	0.1	0.1	$-1, 0, 1$
4	1.76 ~ 176	101	3	5	0.001 ~ 0.1	0.1	0

Other possible origins of the observed sign inversion are SP-ISHE [34], ANE [35], the unidirectional spin Hall magnetoresistance (USMR) [36], and the orbital Hall effect (OHE) [37,38]. These effects reportedly become pronounced at large t_{FM} [39–41]. However, they are discernible from the SI-SOT studied in this work as follows. From the value of spin-mixing conductance between Ta/Co interface, $1.7 \times 10^{-19} \text{ m}^{-2}$, which was estimated from t_{FM} and t_{NM} dependences of the damping coefficient, SP-ISHE was calculated to be less than 15% of S component in our thickness range, which cannot explain the sign inversion (see SM, Secs. A and B [23]) [42–45]. In addition, the sign of S via the ANE and the USMR should be negative [45], which does not rationalize the sign inversion in our Ta/Co. The OHE and resulting torque might also contribute to this phenomenon [37,38]. However, the orbital current injected into the FM layer is rapidly converted into spin current within a thickness of a few atomic layers [37]. In such a case, although the net of spin current injected into the FM layer might be modulated owing to the OHE contribution, its effect is independent of t_{FM} when t_{FM} is thicker than the orbital diffusion length, typically a few atomic layers. This means that the OHE is not responsible for the sign inversion when $t_{\text{FM}} > 10 \text{ nm}$. Therefore, we conclude that the aforementioned effects are negligible.

We also verified the influence of the SI-SOT from the shift of the magnetoresistance curve [46] and the second-harmonic Hall measurements [47,48] (see SM, Secs. C and D [23]). In addition, we confirmed that sign of the magnetoresistance and/or crystalline structure are unchanged even when t_{FM} was increased up to 17.5 nm (see SM, Secs. E and F [23]). Furthermore, we observed sign inversion of ξ_{FMR} due to the SI-SOT in Pt/Fe bilayer (see SM, Sec. G [23]). These control experiments also support our claim that the sign inversion of S in the thick FM is attributed to the enhancement of the SI-SOT. We note that even when the SOT in a single FM layer [31,49–51] is negligibly small, as is previously reported and actually obtained in our single Co layer (see SM, Sec. H [23]), the contribution of the SI-SOT is not negligible because the spin-current absorption to the adjacent NM layer is essential for generation of the SI-SOT.

VI. OVERESTIMATION OF SPIN HALL ANGLE OF NONMAGNETIC MATERIALS DUE TO CONTRIBUTION OF SELF-INDUCED SPIN-ORBIT TORQUES

Finally, we generalize the discussion of ξ_{FMR} to a wide variety of bilayer systems investigated in recent SOT studies. The nonlinear relationships between $1/\xi_{\text{FMR}}$ and $1/t_{\text{FM}}$, in principle, negate the validity of the conventional estimation of ξ_{FL} from linear fitting of the $1/\xi_{\text{FMR}}-1/t_{\text{FM}}$ curve because the SI-SOT is non-negligible. We also emphasize that observing a linear relationship in the $1/\xi_{\text{FMR}}-1/t_{\text{FM}}$ curve does not always mean the absence of SI-SOI, and reliability of estimating ξ_{FL} from linear fitting is a little subtle. To discuss this uncertainty, we calculate $1/\xi_{\text{FMR}}-1/t_{\text{FM}}$ curves for different values of $\xi_{\text{FL}}/\xi_{\text{DL}}$ in Fig. 4(a), where $1/\xi_{\text{FMR}}$ has almost a linear relation to $1/t_{\text{FM}}$ even for $\xi_{\text{FL}}/\xi_{\text{DL}} = 0$. In this case, the value of ξ_{FL} estimated via conventional analysis is nonzero but significantly deviates from the real value, $\xi_{\text{FL}} = 0$, unless SI-SOT is considered. Further model calculation reveals substantial

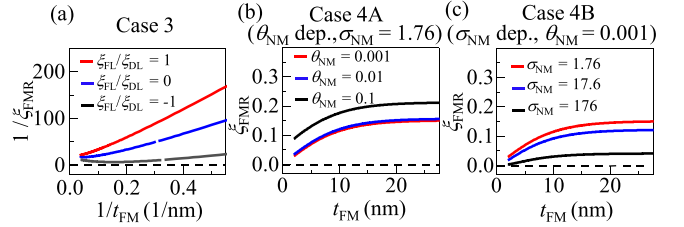


FIG. 4. (a) $\xi_{\text{FL}}/\xi_{\text{DL}}$ dependence of the $1/\xi_{\text{FMR}}-1/t_{\text{FM}}$ curve for case 3. (b) θ_{NM} and (c) σ_{NM} dependences of the $\xi_{\text{FMR}}-t_{\text{FM}}$ curve for case 4. The parameters for $\xi_{\text{FL}}/\xi_{\text{DL}}$, θ_{NM} , and σ_{NM} used in the calculations are shown in each graph. The parameter units are the same as those of Table I.

overestimation of the SHA when the SI-SOT is neglected. Case 4A shown in Fig. 4(b) is an example of a topological insulator (TI) [7,8] where θ_{NM} is changed from 0.001 to 0.1 and θ_{FM} and σ_{NM} are fixed to 0.1 and $1.76 \times 10^4 (\Omega \text{ m})^{-1}$, respectively, i.e., the weakly conductive NM regime. Importantly, large ξ_{FMR} up to 0.15 was obtained even for $\theta_{\text{NM}} = 0.001$. In the conventional analysis, $\xi_{\text{FMR}} \sim \theta_{\text{NM}}$ has been postulated so far for $\xi_{\text{FL}} \sim 0$. Therefore, the calculated result in Fig. 4(b) indicates that θ_{NM} is overestimated by a factor of about 150 if the SI-SOT is neglected. The overestimation is due to neglecting the current shunting into the FM layer and the resulting SI-SOI even when $J_{\text{c(FM)}} \gg J_{\text{c(NM)}}$. S originates from the dampinglike SOT generated by both the SOT from the NM layer and the SI-SOT. Therefore, both $J_{\text{c(NM)}}$ and $J_{\text{c(FM)}}$ contribute to S . In contrast, A is mainly due to the Oersted field generated by $J_{\text{c(NM)}}$ only. In case 4A, $J_{\text{c(NM)}}$ is much lower than $J_{\text{c(FM)}}$ owing to the much lower conductivity of the NM layer. Hence, ξ_{FMR} , which is equivalent to $S(\sim J_{\text{s(NM)}} + J_{\text{s(FM)}})$ divided by $A(\sim J_{\text{c(NM)}})$, is significantly overestimated. Figure 4(c) shows the calculated result when σ_{NM} is changed (case 4B). The overestimation of ξ_{FMR} becomes pronounced when σ_{NM} is low. Further overestimation is expected at the FM/NM interface with spin-splitting states, such as the TI/FM interface. For a TI/FM interface with considerable spin-momentum locking (SML), the electrons change their momentum at the interface, because the Fermi wave number in the topological surface states is considerably smaller than in the FM layer. As a result, SML enhances spin scattering at the interface, which causes enhanced SI-SOT and overestimation of ξ_{FMR} . The aforementioned overestimation occurs not only in ST-FMR but also in other methods such as SOT magnetization switching [5], the second-harmonic method [52], and shifting of the hysteresis loop [53], because these methods also calculate the SHA by dividing the signal by $J_{\text{c(NM)}}$. Careful attention is strongly needed for a proper understanding of SOT physics in bilayer systems.

VII. CONCLUSION

In summary, we observed anomalous sign reversal of the total SOT in Ta(5)/Co(t_{FM}) bilayers when the Co layer was thicker than 8.5 nm, which was attributed to SI-SOT. Such sign reversal occurs when the SHAs of the NM and FM layers have opposite signs. A theoretical model including the SHE of Co calculated using the spin-diffusion equation well

reproduced the experimental results. This model shows that investigating the SHE in various kinds of NM/FM bilayers and choosing an FM layer with the same signs for θ_{FM} as θ_{NM} achieves efficient SOT action in an NM/FM bilayer. In addition, we found that neglecting the SI-SOT causes overestimation of θ_{NM} by two orders for weakly conductive NM layers. The findings in this study enable more reliable SOT estimation, which contributes to development of spin orbitronics using SOT materials. Furthermore, the significant effect of SI-SOT requires revisiting previous studies claiming high SHAs.

The data that support the findings of this study are available from the corresponding author upon reasonable request.

ACKNOWLEDGMENTS

This work was supported by Japan Society for the Promotion of Science (JSPS) (KAKENHI Grants No. 16H06330, No. 19H02197, No. 20H02607, No. 20K22413, and No. 22H00214), Japan Science and Technology Agency (JST), and Precursory Research for Embryonic Science and Technology (PRESTO) (Grant No. JPMJPR20B2).

-
- [1] Y. K. Kato, R. C. Myers, A. C. Gossard, and D. D. Awschalom, Observation of the spin Hall effect in semiconductors, *Science* **306**, 1910 (2004).
- [2] A. Manchon and S. Zhang, Theory of spin torque due to spin-orbit coupling, *Phys. Rev. B* **79**, 094422 (2009).
- [3] I. M. Miron, G. Gaudin, S. Auffret, B. Rodmacq, A. Schuhl, S. Pizzini, J. Vogel, and P. Gambardella, Current-driven spin torque induced by the Rashba effect in a ferromagnetic metal layer, *Nat. Mater.* **9**, 230 (2010).
- [4] I. M. Miron, K. Garello, G. Gaudin, P. J. Zermatten, M. V. Costache, S. Auffret, S. Bandiera, B. Rodmacq, A. Schuhl, and P. Gambardella, Perpendicular switching of a single ferromagnetic layer induced by in-plane current injection, *Nature (London)* **476**, 189 (2011).
- [5] L. Liu, C.-F. Pai, Y. Li, H. W. Tseng, D. C. Ralph, and R. A. Buhrman, Spin-torque switching with the giant spin Hall effect of tantalum, *Science* **336**, 555 (2012).
- [6] C.-F. Pai, L. Liu, Y. Li, H. W. Tseng, D. C. Ralph, and R. A. Buhrman, Spin transfer torque devices utilizing the giant spin Hall effect of tungsten, *Appl. Phys. Lett.* **101**, 122404 (2012).
- [7] Y. Wang, D. Zhu, Y. Wu, Y. Yang, J. Yu, R. Ramaswamy, R. Mishra, S. Shi, M. Elyasi, K.-L. Teo, Y. Wu, and H. Yang, Room temperature magnetization switching in topological insulator-ferromagnet heterostructures by spin-orbit torques, *Nat. Commun.* **8**, 1364 (2017).
- [8] N. H. D. Khang, Y. Ueda, and P. N. Hai, A conductive topological insulator with large spin Hall effect for ultralow power spin-orbit torque switching, *Nat. Mater.* **17**, 808 (2018).
- [9] Z. C. Zheng, Q. X. Guo, D. Jo, D. Go, L. H. Wang, H. C. Chen, W. Yin, X. M. Wang, G. H. Yu, W. He, H.-W. Lee, J. Teng, and T. Zhu, Magnetization switching driven by current-induced torque from weakly spin-orbit coupled Zr, *Phys. Rev. Res.* **2**, 013127 (2020).
- [10] M. Aoki, E. Shigematsu, M. Matsushima, R. Ohshima, S. Honda, T. Shinjo, M. Shiraishi, and Y. Ando, In-plane spin-orbit torque magnetization switching and its detection using the spin rectification effect at subgigahertz frequencies, *Phys. Rev. B* **102**, 174442 (2020).
- [11] L. Liu, T. Moriyama, D. C. Ralph, and R. A. Buhrman, Spin-Torque Ferromagnetic Resonance Induced by the Spin Hall Effect, *Phys. Rev. Lett.* **106**, 036601 (2011).
- [12] D. MacNeill, G. M. Stiehl, M. H. D. Guimaraes, R. A. Buhrman, J. Park, and D. C. Ralph, Control of spin-orbit torques through crystal symmetry in WTe₂/ferromagnet bilayers, *Nat. Phys.* **13**, 300 (2017).
- [13] A. Tsukahara, Y. Ando, Y. Kitamura, H. Emoto, E. Shikoh, M. P. Delmo, T. Shinjo, and M. Shiraishi, Self-induced inverse spin Hall effect in permalloy at room temperature, *Phys. Rev. B* **89**, 235317 (2014).
- [14] C. Du, H. Wang, F. Yang, and P. C. Hammel, Systematic variation of spin-orbit coupling with d-orbital filling: Large inverse spin Hall effect in 3d transition metals, *Phys. Rev. B* **90**, 140407(R) (2014).
- [15] Y. Omori, E. Sagasta, Y. Niimi, M. Gradhand, L. E. Hueso, F. Casanova, and Y. C. Otani, Relation between spin Hall effect and anomalous Hall effect in 3d ferromagnetic metals, *Phys. Rev. B* **99**, 014403 (2019).
- [16] L. Leiva, S. Granville, Y. Zhang, S. Dushenko, E. Shigematsu, T. Shinjo, R. Ohshima, Y. Ando, and M. Shiraishi, Giant spin Hall angle in the Heusler alloy Weyl ferromagnet Co₂MnGa, *Phys. Rev. B* **103**, L041114 (2021).
- [17] Y. Xu, Y. Yang, K. Yao, B. Xu, and Y. Wu, Self-current induced spin-orbit torque in FeMn/Pt multilayers, *Sci. Rep.* **6**, 26180 (2016).
- [18] K.-W. Kim and K.-J. Lee, Generalized Spin Drift-Diffusion Formalism in the Presence of Spin-Orbit Interaction of Ferromagnets, *Phys. Rev. Lett.* **125**, 207205 (2020).
- [19] H. Ochoa, R. Zarzuela, and Y. Tserkovnyak, Self-induced spin-orbit torques in metallic ferromagnets, *J. Magn. Magn. Mater.* **538**, 168262 (2021).
- [20] T. Valet and A. Fert, Theory of the perpendicular magnetoresistance in magnetic multilayers, *Phys. Rev. B* **48**, 7099 (1993).
- [21] C. Kittel, On the theory of ferromagnetic resonance absorption, *Phys. Rev.* **73**, 155 (1948).
- [22] V. Tshitoyan, C. Ciccarelli, A. P. Mihal, M. Ali, A. C. Irvine, T. A. Moore, T. Jungwirth, and A. J. Ferguson, Electrical manipulation of ferromagnetic NiFe by antiferromagnetic IrMn, *Phys. Rev. B* **92**, 214406 (2015).
- [23] See Supplemental Material at <http://link.aps.org/supplemental/10.1103/PhysRevB.106.174418> for more details on the estimation of the spin-mixing conductance, contribution of spin pumping, control experiments using the shift of the magnetoresistance curve and the second-harmonic Hall measurement, thickness dependence of the magnetoresistance and crystalline structure, ST-FMR measurement for Pt/Fe bilayer, and SOT in a single Co layer.
- [24] H. Hayashi, A. Musha, H. Sakimura, and K. Ando, Spin-Orbit Torques Originating from the Bulk and Interface in Pt-Based Structures, *Phys. Rev. Res.* **3**, 013042 (2021).
- [25] J. Sklenar, W. Zhang, M. B. Jungfleisch, H. Saglam, S. Grudichak, W. Jiang, J. E. Pearson, J. B. Ketterson, and A.

- Hoffmann, Unidirectional spin-torque driven magnetization dynamics, *Phys. Rev. B* **95**, 224431 (2017).
- [26] M. Aoki, E. Shigematsu, R. Ohshima, T. Shinjo, M. Shiraishi, and Y. Ando, Current-induced out-of-plane torques in a single permalloy layer with lateral structural asymmetry, *Phys. Rev. B* **105**, 144407 (2022).
- [27] C.-F. Pai, Y. Ou, L. H. Vilela-Leão, D. C. Ralph, and R. A. Buhrman, Dependence of the efficiency of spin Hall torque on the transparency of Pt/ferromagnetic layer interfaces, *Phys. Rev. B* **92**, 064426 (2015).
- [28] R. Suzuki, S. Haku, H. Hayashi, and K. Ando, Spin-torque ferromagnetic resonance in electrochemically etched metallic device, *Appl. Phys. Express* **13**, 043007 (2020).
- [29] A. Manchon, R. Matsumoto, H. Jaffres, and J. Grollier, Spin transfer torque with spin diffusion in magnetic tunnel junctions, *Phys. Rev. B* **86**, 060404(R) (2012).
- [30] J. Zhang, P. M. Levy, S. Zhang, and V. Antropov, Identification of Transverse Spin Currents in Noncollinear Magnetic Structures, *Phys. Rev. Lett.* **93**, 256602 (2004).
- [31] W. Wang, T. Wang, V. P. Amin, Y. Wang, A. Radhakrishnan, A. Davidson, S. R. Allen, T. J. Silva, H. Ohldag, D. Balzar, B. L. Zink, P. M. Haney, J. Q. Xiao, D. G. Cahill, V. O. Lorenz, and X. Fan, Anomalous spin-orbit torques in magnetic single-layer films, *Nat. Nanotechnol.* **14**, 819 (2019).
- [32] E. Montoya, P. Omelchenko, C. Coutts, N. R. Lee-Hone, R. Hübner, D. Broun, B. Heinrich, and E. Girt, Spin transport in tantalum studied using magnetic single and double layers, *Phys. Rev. B* **94**, 054416 (2016).
- [33] V. P. Amin, J. Li, M. D. Stiles, and P. M. Haney, Intrinsic spin currents in ferromagnets, *Phys. Rev. B* **99**, 220405(R) (2019).
- [34] K. Ando, S. Takahashi, J. Ieda, Y. Kajiwara, H. Nakayama, T. Yoshino, K. Harii, Y. Fujikawa, M. Matsuo, S. Maekawa, and E. Saitoh, Inverse spin-Hall effect induced by spin pumping in metallic system, *J. Appl. Phys.* **109**, 103913 (2011).
- [35] A. v. Etingshausen and W. Nernst, Ueber das auftreten electromotorischer kräfte in metallplatten, welche von einem wärmestrome durchflossen werden und sich im magnetischen felde befinden, *Ann. Phys.* **265**, 343 (1886).
- [36] C. O. Avci, K. Garello, A. Ghosh, M. Gabureac, S. F. Alvarado, and P. Gambardella, Unidirectional spin Hall magnetoresistance in ferromagnet/normal metal bilayers, *Nat. Phys.* **11**, 570 (2015).
- [37] D. Go and H.-W. Lee, Orbital torque: Torque generation by orbital current injection, *Phys. Rev. Res.* **2**, 013177 (2020).
- [38] D. Go, F. Freimuth, J.-P. Hanke, F. Xue, O. Gomonay, K.-J. Lee, S. Blügel, P. M. Haney, H.-W. Lee, and Y. Mokrousov, Theory of current-induced angular momentum transfer dynamics in spin-orbit coupled systems, *Phys. Rev. Res.* **2**, 033401 (2020).
- [39] K. Kondou, H. Sukegawa, S. Kasai, S. Mitani, Y. Niimi, and Y. Otani, Influence of inverse spin Hall effect in spin-torque ferromagnetic resonance measurements, *Appl. Phys. Express* **9**, 023002 (2016).
- [40] S. Karimeddiny, J. A. Mittelstaedt, R. A. Buhrman, and D. C. Ralph, Transverse and Longitudinal Spin-Torque Ferromagnetic Resonance for Improved Measurement of Spin-Orbit Torque, *Phys. Rev. Appl.* **14**, 024024 (2020).
- [41] Q. Liu, Y. Zhang, L. Sun, B. Miao, X. R. Wang, and H. F. Ding, Influence of the spin pumping induced inverse spin Hall effect on spin-torque ferromagnetic resonance measurements, *Appl. Phys. Lett.* **118**, 132401 (2021).
- [42] J. M. Shaw, H. T. Nembach, and T. J. Silva, Determination of spin pumping as a source of linewidth in sputtered Co₉₀Fe₁₀/Pd multilayers by use of broadband ferromagnet, *Phys. Rev. B* **85**, 054412 (2012).
- [43] L. Zhu, D. C. Ralph, and R. A. Buhrman, Effective Spin-Mixing Conductance of Heavy-Metal-Ferromagnet Interfaces, *Phys. Rev. Lett.* **123**, 057203 (2019).
- [44] L. Zhu, L. Zhu, D. C. Ralph, and R. A. Buhrman, Origin of Strong Two-Magnon Scattering in Heavy-Metal/Ferromagnet/Oxide Heterostructures, *Phys. Rev. Appl.* **13**, 034038 (2020).
- [45] M. Aoki, E. Shigematsu, R. Ohshima, T. Shinjo, M. Shiraishi, and Y. Ando, Coexistence of low-frequency spin-torque ferromagnetic resonance and unidirectional spin Hall magnetoresistance, *Phys. Rev. B* **104**, 094401 (2021).
- [46] Y.-T. Liu, T.-Y. Chen, T.-H. Lo, T.-Y. Tsai, S.-Y. Yang, Y.-J. Chang, J.-H. Wei, and C.-F. Pai, Determination of Spin-Orbit-Torque Efficiencies in Heterostructures with In-Plane Magnetic Anisotropy, *Phys. Rev. Appl.* **13**, 044032 (2020).
- [47] C. O. Avci, K. Garello, M. Gabureac, A. Ghosh, A. Fuhrer, S. F. Alvarado, and P. Gambardella, Interplay of spin-orbit torque and thermoelectric effects in ferromagnet/normal-metal bilayers, *Phys. Rev. B* **90**, 224427 (2014).
- [48] Y. Du, R. Thompson, M. Kohda, and J. Nitta, Origin of spin-orbit torque in CoFeB single-layer CoFeB investigated via in-plane harmonic Hall measurements, *AIP Adv.* **11**, 025033 (2021).
- [49] L. Zhu, D. C. Ralph, and R. A. Buhrman, Unveiling the mechanism of bulk spin-orbit torques within chemically disordered Fe_xPt_{1-x} single layers, *Adv. Funct. Mater.* **31**, 2103898 (2021).
- [50] T. Seki, Y.-C. Lau, S. Iihama, and K. Takanashi, Spin-orbit torque in a Ni-Fe single layer, *Phys. Rev. B* **104**, 094430 (2021).
- [51] Q. Fu, L. Liang, W. Wang, L. Yang, K. Zhou, Z. Li, C. Yan, L. Li, H. Li, and R. Liu, Observation of nontrivial spin-orbit torque in single-layer ferromagnetic metals, *Phys. Rev. B* **105**, 224417 (2022).
- [52] Y. Fan, P. Upadhyaya, X. Kou, M. Lang, S. Takei, Z. Wang, J. Tang, L. He, L. Te Chang, M. Montazeri, G. Yu, W. Jiang, T. Nie, R. N. Schwartz, Y. Tserkovnyak, and K. L. Wang, Magnetization switching through giant spin-orbit torque in a magnetically doped topological insulator heterostructure, *Nat. Mater.* **13**, 699 (2014).
- [53] C.-F. Pai, M. Mann, A. J. Tan, and G. S. D. Beach, Determination of spin torque efficiencies in heterostructures with perpendicular magnetic anisotropy, *Phys. Rev. B* **93**, 144409 (2016).